Biosensors and Bioelectronics 49 (2013) 25–31

Contents lists available at SciVerse ScienceDirect

Biosensors and Bioelectronics

journal homepage: www.elsevier.com/locate/bios

# Acetylcholinesterase biosensor based on $SnO_2$ nanoparticles–carboxylic graphene–nafion modified electrode for detection of pesticides

Long Yang [a], Qing Zhou [b], Guangcan Wang [a,*], Yun Yang [c]

[a] School of Chemical Science and Engineering, Yunnan University, 2 North Cuihu Road, Kunming 650091, PR China
[b] School of Physical Science and Technology, Yunnan University, Kunming 650091, China
[c] Division of Electron Microscopy, Kunming Medical University, Kunming 650500, China

ARTICLE INFO

*Article history:*
Received 17 March 2013
Accepted 22 April 2013
Available online 2 May 2013

*Keywords:*
$SnO_2$ nanoparticle
Carboxylic graphene
Acetylcholinesterase
Amperometric biosensor
Stability

ABSTRACT

A sensitive amperometric acetylcholinesterase (AChE) biosensor, based on $SnO_2$ nanoparticles ($SnO_2$ NPs), carboxylic graphene (CGR) and nafion (NF) modified glassy carbon electrode (GCE) for the detection of methyl parathion and carbofuran has been developed. The nanocomposites of $SnO_2$ NPs and CGR was synthesized and characterized by scanning electron microscopy (SEM), X-ray diffraction (XRD) and Fourier transform infrared spectroscopy (FTIR), respectively. Chitosan (CS) was used to immobilize AChE on $SnO_2$ NPs–CGR–NF/GCE and to improve electronic transmission between AChE and $SnO_2$ NPs–CGR–NF/GCE. NF was used as the protective membrane for the AChE biosensor. The $SnO_2$ NPs–CGR–NF nanocomposites with excellent conductivity, catalysis and biocompatibility offered an extremely hydrophilic surface for AChE adhesion. The AChE biosensor showed favorable affinity to acetylthiocholine chloride (ATCl) and could catalyze the hydrolysis of ATCl with an apparent Michaelis–Menten constant value of 131 μM. The biosensor detected methyl parathion in the linear range from $10^{-13}$ to $10^{-10}$ M and from $10^{-10}$ to $10^{-8}$ M. The biosensor detected carbofuran in the linear range from $10^{-12}$ to $10^{-10}$ M and from $10^{-10}$ to $10^{-8}$ M. The detection limits of methyl parathion and carbofuran were $5 \times 10^{-14}$ M and $5 \times 10^{-13}$ M, respectively. The biosensor exhibited low applied potential, high sensitivity and acceptable stability, thus providing a promising tool for analysis of pesticides.



## 1. Introduction

Pesticides have played an important role in increasing agricultural productivity. They are still extensively used up to now. Because of their high toxicity and widespread use in agriculture, the residue could be left in the environment. Owing to their bioaccumulation effect, they can cause long-term damage to both the environment and lives even though their concentration is very low (Videira et al., 2001). Therefore, the quantitative detection of pesticides is quite significant. Biosensors based on AChE have emerged as a promising technique for toxicity analysis, environmental monitoring, food quality control and military investigations in recent years (Hosea et al., 1995; Andreescu and Marty, 2006). The main application of AChE biosensors is for the detection of organophosphate and carbamate pesticides based on enzyme inhibition. These devices are designed to complement or replace the existing reference analytical methods such as HPLC, GC, GC/MS etc. by simplifying or eliminating sample preparation, thus decreasing the analysis time and cost. However, so far, the detection limits of AChE biosensors cannot reach the same level of those analysis instruments. In addition, in order to immobilize enzyme, large amounts of chemical reagents were used, resulting in the loss of enzyme activity. Our research purpose is to develop a sensitive and stable AChE biosensor in a simple and green way for detection of pesticides.

Graphene, a two-dimensional sheet of sp2-bonded carbon atoms arranged in a honeycomb lattice, has attracted increasing attention since it was first isolated from three-dimensional graphite by mechanical exfoliation (Novoselov et al., 2004). Due to its extraordinary thermal, mechanical, and electrical properties, graphene is usually considered as a competitive candidate for next-generation electronic application devices such as supercapacitors (Stoller et al., 2008; Mishra and Ramaprabhu, 2011), batteries (Yoo et al., 2008; Xiao et al., 2011), fuel cells (Seger and Kamat, 2009; Kou et al., 2009), solar cells (Wang et al., 2008; Wu et al., 2008), sensors (Guo and Dong, 2011; Yang et al., 2009), biosensors (Wang et al., 2011a; Qiu et al., 2011), energy storage (Chen et al., 2010) and catalysts (Han et al., 2011; Nie et al., 2012), etc. However, many

* Corresponding author. Tel.: +86 871 5033218; fax: +86 871 5153832.
*E-mail address:* wangc166163@sina.com (G. Wang).

0956-5663/$ - see front matter © 2013 Elsevier B.V. All rights reserved.
http://dx.doi.org/10.1016/j.bios.2013.04.037

researches have reported that the pure graphene actually exhibit unsatisfactory electrical conductivity because of the inevitable aggregation (Stankovich et al., 2006; Li and Kaner, 2008). On the contrary, functionalized graphene sheets are easier to disperse in organic solvents, which can improve the dispersion and homogeneity of the graphene within the polymer and yield novel types of electrically conductive nanocomposites (Stankovich et al., 2006; Li and Kaner, 2008; Wang et al., 2011b). Besides, some of the useful and unique properties of graphene can only be realized after it is functionalized with organic groups such as hydroxyl, carboxyl, amino and the like (Sheng et al., 2011; Zheng et al., 2012; Chen et al., 2012).

Nanostructural metal oxide semiconductors possess high surface area, nontoxicity, good biocompatibility, catalytic activity and chemical stability. Among the metal oxide semiconductors, tin oxide ($SnO_2$), an n-type semiconductor with a wide band gap of 3.6 eV at 300 K, has been investigated for various applications such as solar cells, electrochemistry sensors and biosensor (Chappel and Zaban, 2002; Fuchs et al., 2011; Patil et al., 2007; Korotcenkov et al., 2009; Chu et al., 2011; Mahadeva and Kim, 2011; Li et al., 2010).

In recent years, the nanocomposites of $SnO_2$ NPs and carbon nanomaterials showed better electrochemical performance than the pure $SnO_2$ (Wen et al., 2007; Kim et al., 2010). They have been applied in the investigation fields of electrochemistry such as lithium-ion battery and supercapacitor with finer catalysis and electrical conductivity characteristics (Han et al., 2010; Yao et al., 2009; Lu et al., 2010). However, many of the interesting and unique properties of the nanocomposite can only be realized after it is integrated into more complex assemblies (Stankovich et al., 2006; Li and Kaner, 2008).

CS is an abundant natural biopolymer with excellent film forming ability, biocompatibility, and nontoxicity. It provides natural microenvironment to the enzyme and also gives sufficient accessibility to electrons to shuttle between the enzyme and the electrode. AChE immobilized by CS can keep high enzyme activity and improves electrons transmission between the enzyme and modified electrode. NF polymer is chemically inert, ideal conductivity, hydrophilic, and insoluble in water, and thus possesses almost ideal properties for preparation of modified electrodes (Hu et al., 1998). Incorporation of some nanomaterials with high conductivity and catalytic activity, NF seems to be a possible approach to improve the sensitivity, selectivity and stability of modified electrodes. The NF–graphene nanocomposite film modified electrode for determination of cadmium presented high sensitivity (Li et al., 2009). Nanosilver–NF modified electrode for electrochemical detection of methyl parathion showed strong electrocatalytic activity, good stability and reproducibility (Kumaravel and Chandrasekaran, 2010). Horseradish peroxidase biosensor based on NF–graphene modified electrode for determination of $H_2O_2$ exhibited both good operational storage and storage stability (Li et al., 2011).

Motivated by these reports, herein, we developed a sensitive amperometric AChE biosensor based on $SnO_2$ NPs, CGR and NF modified GCE for the detection of methyl parathion and carbofuran. The $SnO_2$ NPs–CGR nanocomposite was homogeneously dispersed in NF. The nanocomposite film of $SnO_2$ NPs–CGR–NF was effectively fastened on the modified electrode. CS was used to immobilize the AChE on $SnO_2$ NPs–CGR–NF/GCE and to improve electronic transmission between AChE and $SnO_2$ NPs–CGR–NF/GCE. NF was used as the protective membrane for the AChE biosensor. The high sensitivity and stability of the modified electrode were attributed to the synergistic effects of their excellent electric conductivity, large surface area and electrocatalytic activity of $SnO_2$ NPs, CGR and NF. The AChE biosensor displayed high enzyme activity and favorable affinity to ATCl, high catalytic activity to the hydrolysis of ATCl and high electrochemistry response. The stable and sensitive biosensor might be an effective device for detection of pesticides.

This study provided a universal and effective enzyme immobilization platform for meeting the demand of the effective immobilization enzyme on the electrode surface. The biosensor showed high sensitivity, acceptable stability and reproducibility for the analysis of acetylcholine and pesticides.

## 2. Material and methods

### 2.1. Reagents

ATCl, AChE (Type C3389, 500 U/mg from electric eel), CS (85% deacetylation), NF (5% in lower aliphatic alcohols and water) were purchased from Sigma-Aldrich (St. Louis, USA). Methyl parathion and carbofuran were obtained from China's Agriculture Ministry (Beijing China). Graphite powder was purchased from Sinopharm Chemical Reageat Company. (China). $SnCl_2 \cdot 2H_2O$ was obtained from Shanghai Chemical Reagent Co. Ltd. (China). All other reagents were of analytical grade. Aqueous solutions were prepared with deionized (DI) water (18 MΩ cm).

### 2.2. Apparatus

The electrochemical measurements were carried out on an IM6ex electrochemical workstation (Zahner Elektrik Instruments, Germany). A conventional three-electrode system was employed with a saturated calomel electrode (SCE) as the reference electrode, a platinum foil as the counter electrode, and the modified GCE (diameter = 3 mm) as the working electrodes. Cyclic voltammetry (CV) measurements were performed in 0.1 M of phosphate buffer solution (PBS, pH 7.4). All experiments were performed at room temperature ($25 \pm 1$°C). CGR and $SnO_2$ NPs–CGR nanocomposites were characterized by scanning electron microscopy (SEM, QUNT200 USA), Fourier transform infrared spectrometry (FTIR, Thermo Fisher SCIENTIFIC Nicolet IS10 USA) and X-ray diffractometer (XRD, Rigaku TTR III, Japan).

### 2.3. Preparation of CGR

Graphite oxide prepared by Hummers' method (Hummers and Offeman, 1958) was suspended in water and exfoliated through ultrasonication (2 h) to obtain graphene oxide (GO) solution. GO solution was centrifuged at 3000 rpm to remove unexfoliated graphite oxide. CGR was prepared by a chemical method. Briefly, GO aqueous suspension (5 ml) was diluted as to give a concentration of 2.0 mg/ml, and then sonicated for 1 h to give a clear solution. 1.2 g of NaOH and 1.0 g of chloroacetic acid (Cl–$CH_2$–COOH) were added to the suspension and sonicated for 3 h to convert the –OH groups to –COOH via conjugation of acetic acid moieties. Sequentially the suspension was separated by centrifuging at a speed of 15,000 rpm, washed with DI water for several cycles, dried in an oven at 60 °C to gain CGR (Sun et al., 2008).

### 2.4. Synthesis $SnO_2$ NPs–CGR nanocomposites

The $SnO_2$ NPs–CGR was prepared as follows: 2.0 mg of CGR were suspended in 100 μl of 0.01 M $SnCl_2 \cdot 2H_2O$ by sonicating for 10 min to disperse CGR equably in $SnCl_2 \cdot 2H_2O$ solution. After 100 μl of 0.01 M of sodium citrate, 10.0 ml of ethanol and 20.0 ml of DI water were added to the suspension; ice-cold, freshly prepared 120 μl of 0.05 M $NaBH_4$ solution was then added to the above mixture and until the color of the solution did not change. The suspension was separated by centrifuging at a speed of

12,000 rpm, washed with DI water for several cycles, dried in an oven at 60 °C. Then Sn NPs were oxidized to $SnO_2$ NPs by heating at 300 °C in atmosphere.

### 2.5. Preparation of AChE biosensor

NF solution (0.125%, Wt/V) was prepared by diluting 5% of NF with ethanol and DI water (V/V, 1/1). The $SnO_2$ NPs–CGR (0.5 mg) were added to 1.0 ml of NF solution and sonicated thoroughly until a homogeneous suspension of $SnO_2$ NPs–CGR–NF was obtained. Similarly 0.5 mg/ml CGR–NF and 0.5 mg/ml GO–NF homogeneous suspension was obtained. The suspension was stored under refrigeration 4 °C.

A GCE was polished carefully to a mirror-like with 0.3 and 0.05 μm alumina slurry and sequentially sonicated for 3 min in ethanol and water. Before the experiment, the electrode was scanned from −0.1 to + 1.1 V until a steady-state current–voltage curve was obtained in PBS (pH7.4). The $SnO_2$ NPs–CGR–NF/GCE was prepared by casting 5 μl of the 0.5 mg/ml $SnO_2$ NPs–CGR–NF suspension onto the GCE and drying at room temperature. A similar casting procedure was used to prepare CGR–NF/GCE and GO–NF/GCE.

The enzyme solution was mixed as 0.05 U AChE and 0.2% CS ($W_t$/V, 50 mM acetic acids). The modified electrodes were each coated 4.5 μl of AChE–CS (V/V, 2/1) and dried overnight at 4 °C. The modified electrodes were washed with PBS (pH 7.4) to remove the unbound AChE. Finally, these biosensors were each covered with 3 μl of 0.1% ($W_t$/V) NF as the protective membrane and then stored at 4 °C. Thus, the three structures of biosensor were: NF/AChE–CS/GO–NF/GCE, NF/AChE–CS/CGR–NF/GCE and NF/AChE–CS/$SnO_2$ NPs–CGR–NF/GCE. As a control, NF/AChE–CS/GCE was also produced.

### 2.6. Detection of ATCl

The typical current–time CV plot for the biosensor was gained at 0.47 V after the successive addition of ATCl to PBS with stirring. The apparent Michaelis–Menten constant ($K_m^{app}$) of the biosensor was calculated from the Lineweaver–Burk equation

$$\frac{1}{i_{ss}} = \left(\frac{K_m^{app}}{i_{max}}\right)\left(\frac{1}{C}\right) + \left(\frac{1}{i_{max}}\right) \quad (1)$$

where $i_{ss}$ is the steady-state current after the addition of substrate, $i_{max}$ is the maximum current measured under saturated substrate condition and $C$ is the concentration of the substrate. The $K_m^{app}$ value, which gives an indication of the enzyme substrate kinetics for the biosensor, was determined by analysis of the slope and intercept for the plot of the reciprocals of the steady-state current versus ATCl concentration.

### 2.7. Effect of incubation time

Inhibition of methyl parathion and carbofuran were tested by CV in terms of their effect on AChE activity at different incubation times (2–20 min) in a pesticide solution ($10^{-10}$ M).

### 2.8. Detection of pesticides

The NF/AChE–CS/$SnO_2$ NPs–CGR–NF/GCE was first immersed in PBS (pH7.4) containing different concentrations of standard pesticide at room temperature (25 ± 1 °C) for 6 min and then transferred to the electrochemical cell of PBS containing 0.5 mM ATCl to study the amperometric response by CV between 0.0 V and 1.0 V. The inhibition of pesticide was calculated as follows:

$$\text{inhibition } (\%) = \frac{i_{P,control} - i_{P,exp}}{i_{P,control}} \times 100\% \quad (2)$$

where $i_{p,control}$ is the peak current of ATCl on NF/AChE–CS/$SnO_2$ NPs–CGR/GCE, $i_{p,exp}$ is the amperometric response of ATCl on NF/AChE–CS/$SnO_2$ NPs–CGR/GCE with pesticide inhibition.

### 2.9. Interference study

The interfering species of glucose (0.5 mM), citric acid (0.5 mM), oxalic acid (0.5 mM), $PO_4^{3-}$ (0.5 mM), $SO_4^{2-}$ (0.5 mM), $NO_3^-$ (0.5 mM), Cu(II) (0.5 mM), Pb(II) (0.5 mM), Hg(II) (0.5 mM), 0.5 mM of p-nitrophenol, 0.5 mM of nitrobenzene, 0.5 mM of p-nitroaniline, 0.5 mM of trinitrotoluene, 0.5 mM of toluene and 0.5 mM of p-toluenesulfonic acid were studied. The signal for a 0.5 mM ATCl was compared with the signal obtained in the presence of the interfering species after incubated by $10^{-10}$ M methyl parathion.

### 2.10. Repeatability, reproducibility and stability studies

The intra-assay precision of the biosensor was evaluated by testing one NF/AChE–CS/$SnO_2$ NPs–CGR–CS/GCE for six times in 0.5 mM ATCl after being immersed in the $1.0 \times 10^{-10}$ M methyl parathion for 6 min. The inter-assay precision was estimated with six different biosensors in the same way.

Stability was evaluated by testing the amperometric response of the NF/AChE–CS/$SnO_2$ NPs–CGR–CS/GCE biosensor in 0.1 M PBS containing 0.5 mM ATCl by CV every five days.

### 2.11. Preparation and determination of real samples

The apple and cabbage samples were obtained from local market in Kunming City. Briefly, the apple and cabbage were cleaned and mashed to pulp with a blender, then two sorts of 25.0 g pulp were mixed with 50 ml acetonitrile and proper amount of 0.1 M NaCl, respectively, and the organic phases were collected and evaporated on a steam bath. The final volume was adjusted to 5.0 ml by adding appropriate amount of dichloromethane. Part of the sample solution was transferred to 0.1 M PBS (pH 7.4) for determination. The water sample (lake water) was filtered through a 0.22 μm membrane and the pH was adjusted to 7.4. After simple pretreatment, different concentrations of methyl parathion and carbofuran were added to study the recovery under the optimal conditions.

## 3. Results and discussion

### 3.1. Characterization of $SnO_2$ NPs–CGR

FTIR result for the CGR was shown in Fig. 1A. The appearance of strong peaks at 3424 $cm^{-1}$ and 1727 $cm^{-1}$ confirmed the presence of the carboxylic group. The X-ray diffraction pattern of the $SnO_2$ NPs–CGR nanocomposites was showed in Fig. 1B. The major diffraction lines were indexed to the tetragonal rutile $SnO_2$ phase. The broad diffraction peaks of the $SnO_2$ indicated small crystal size. The general morphology of the $SnO_2$ NPs–CGR nanocomposites was observed by SEM in Fig. 1C. It showed that $SnO_2$ NPs were embedded in the curly CGR nanosheets.

### 3.2. Electrochemical behavior of the biosensors

CV of ATCl and enzymatic product thiocholine were investigated on four different biosensors: NF/AChE–CS/GCE; NF/AChE–CS/GO–NF/GCE; NF/AChE–CS/CGR–NF/GCE and NF/AChE–CS/$SnO_2$ NPs–CGR–NF/GCE. As shown in Fig. 2, no amperometric response was observed

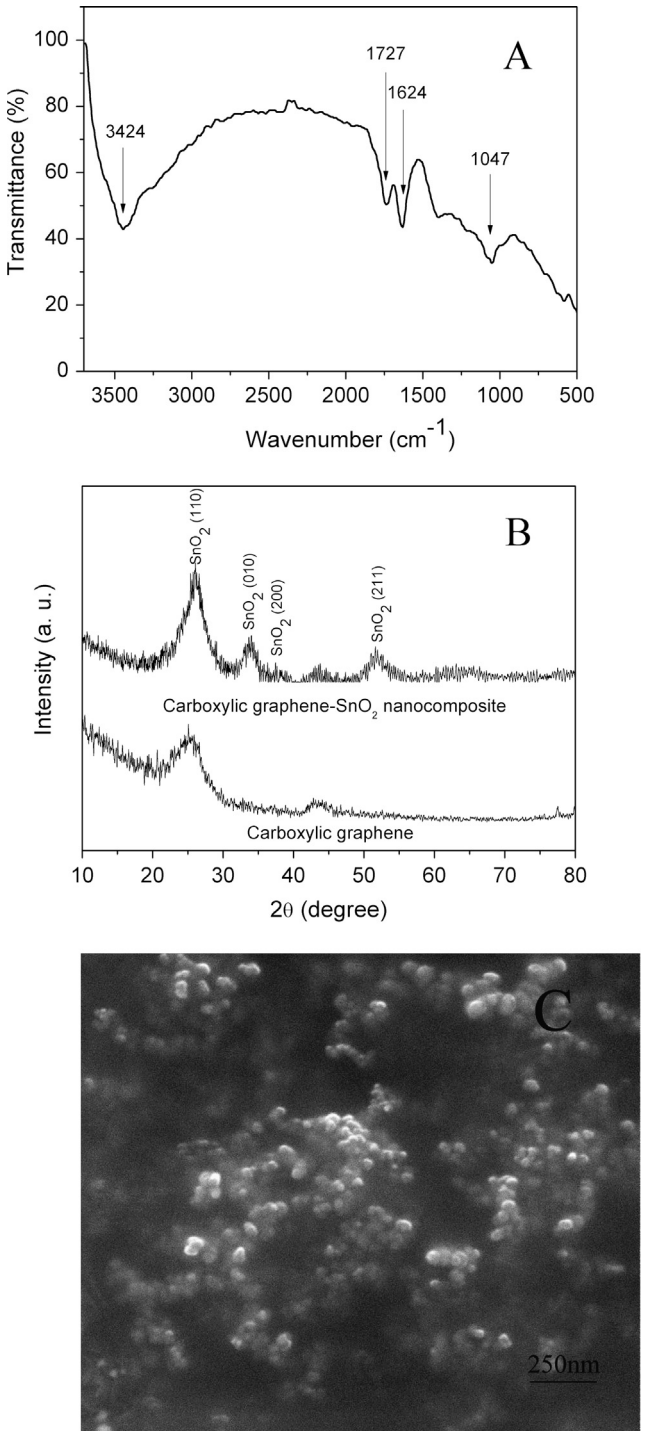


**Fig. 1.** (A) FTIR spectrum of CGR; (B) XRD patterns of CGR and $SnO_2$ NPs–CGR and (C) SEM image of $SnO_2$ NPs–CGR.

for all biosensors in only PBS (curve a–d). However, when 0.5 mM ATCl was added into the PBS, obvious amperometric responses were observed for all of them (curves e–h). The oxidation peak currents increased and the oxidation peak potentials shifted negatively in sequence. At the NF/AChE–CS/$SnO_2$ NPs–CGR–NF/GCE biosensor, the oxidation peak current was the highest and peak potential was the lowest of four biosensors (curve h). It indicated that $SnO_2$ NPs–CGR could greatly improve electron transfer and catalysis which increased peak current and decreased the potential, which was beneficial for avoiding interference from other electroactive species in biological

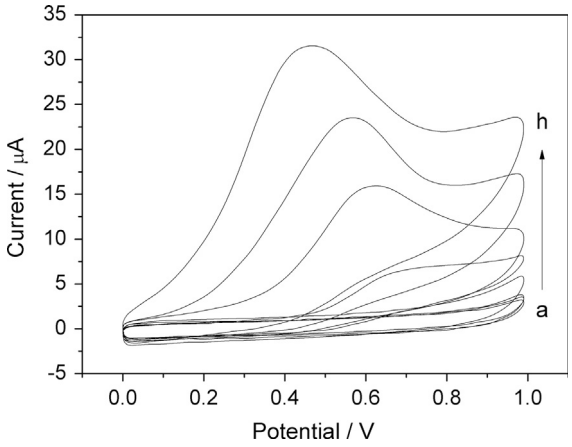


**Fig. 2.** CV of NF/AChE–CS/GCE (a), NF/AChE–CS/GO–NF/GCE (b), NF/AChE–CS/CGR–NF/ GCE (c), NF/AChE–CS/$SnO_2$ NPs–CGR–NF/GCE (d) in 0.1 M PBS and in 0.1 M PBS containning 0.5 mM ATCl (e–h), Scan rate: 0.10 V/s in 25 °C.

matrix. Obviously, $SnO_2$ NPs–CGR–NF/GCE with excellent conductivity and catalytic activity provided an extremely hydrophilic surface for AChE adhesion. Besides, NF protective membrane was used to prevent the loss of the enzyme molecules, improve the anti-interference ability of the biosensor and provide a biocompatible microenvironment to maintain enzymatic activity.

### 3.3. Optimization of the preparation of the biosensor

Optimization of volume of NiO NPs–CGR–NF, ratio of NiO NPs in NiO NPs–CGR and amount of immobilized AChE were supplied in Supplementary materials.

In order to enhance the stability of the biosensor, CS was used to immobilize the AChE on $SnO_2$ NPs–CGR–NF/GCE and to improve electronic transmission between AChE and $SnO_2$ NPs–CGR–NF/GCE. NF was used as the protective membrane for the AChE biosensor. The NF/AChE–CS/$SnO_2$NPs–CGR–NF/GCE (a), AChE–CS/$SnO_2$NPs–CGR–NF/GCE (b) and AChE/$SnO_2$NPs–CGR–NF/GCE (c) biosensors were continuously tested six times in PBS (pH 7.4) containing 0.5 mM ATCl (Fig. S4). The RSD of amperometric response of theirs was 2.58% (a), 6.85% (b), 12.57% (c), respectively. The results showed that the CS immobilized AChE and NF protective membrane effectively improved stability of the AChE biosensor.

The bioactivity of the immobilized AChE depends on the pH of the ATCl solution. The relationship between amperometric responses of AChE with the pH of the ATCl solution was showed in Fig. S5. In the pH range from 6.8 to 8.0, the amperometric response increased with increasing pH and reached a maximum at 7.4. The further increase in the pH of solution led to an obvious decrease of the amperometric response. Therefore, pH 7.4 was used in the detection solution.

The effect of the PBS concentration was also studied as shown in Fig. S6. The experimental results showed that the amperometric response was not enough stable with the PBS concentration at the range of 0.01–0.1 M PBS (7.4) and the amperometric response decreased with the increasing of the PBS concentration at the range of 0.1–0.5 M. The decrease of the signal was probably attributed to the leaking of AChE from the electrode surface. The AChE was removed under higher salinity conditions (Liu and Lin, 2006). Therefore, 0.1 M PBS (pH 7.4) was employed in this work.

### 3.4. Detection of ATCl at NF/AChE–CS/$SnO_2$ NPs–CGR–NF/GCE biosensor

Under the optimized experimental conditions, the AChE biosensor was explored by CV measurements. Fig. 3A showed the

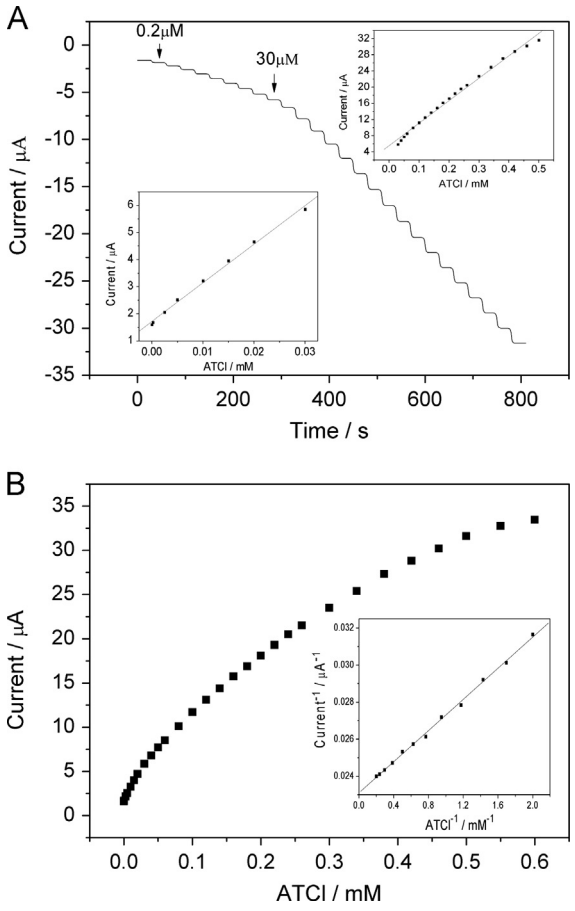


**Fig. 3.** (A) Typical current–time plot for the sensor on successive addition of stock ATCl to 0.1 M PBS, insets show the calibration curves for ATCl determination and (B) calibration plot for the ATCl sensor, inset shows the Lineweaver–Burk plot of $1/i_{ss}$ versus $1/C$.

amperometric response at the NF/AChE–CS/$SnO_2$ NPs–CGR–NF/GCE at 0.47 V in a stirred solution, to which was added an ATCl stock solution. With the increasing of ATCl concentration, the amperometric response of the biosensor increased. The amperometric response of the biosensor was a linear function of ATCl concentration in two segments. One was from 0.2 μM to 30 μM; the other was from 30 μM to 500 μM. The two linear ranges indicated that the linear range of AChE biosensors for acetylcholine was approximately two orders of magnitude. When the concentration of ATCl was saturated, the amperometric response gradually tended to a constant value. The detection limit was 0.1 μM. For higher ATCl concentrations the shape of the amperometric response was indicative of a Michaelis–Menten process (Fig. 3B). The $K_m^{app}$ in the present studies was calculated to be 131 μM according to Lineweaver–Burk equation. This value was lower than that of 240 μM (Wang K. et al., 2011) and 300 μM (Chu et al., 2011) reported by literatures.

### 3.5. Effect of incubation time

The residual activity of the enzyme is influenced by the incubation time of the AChE to pesticides. When the incubation time was longer than 10 min, the curves of inhibitions tended to a stable value, indicating the binding interaction between pesticides and active target groups in the enzyme reaches saturation (Fig. S7). Considering the whole analytical time, sensitivity and stability of the biosensor, 6 min was selected as the optimum incubation time.

### 3.6. Detection of pesticides

After incubation with different concentration methyl parathion, amperometric response of the biosensor was determined by CV as shown in Fig. 4A. The calibration plots of inhibition percentage versus pesticides concentration were showed in Fig. 4B. Linear equations of methyl parathion are $I(\%)=112.13+6.56\ \log C$ from $10^{-13}$ to $10^{-10}$ M with a correlation coefficient of 0.9961 and $I(\%)=71.21+2.48\ \log C$ from $10^{-10}$ to $10^{-8}$ M with a correlation coefficient of 0.9967. Linear equations of carbofuran were $I(\%)=182.15+13.59\ \log C$ from $10^{-12}$ to $10^{-10}$ M with a correlation coefficient of 0.9957 and $I(\%)=78.37+3.17\ \log C$ from $10^{-10}$ to $10^{-8}$ M with a correlation coefficient of 0.9965. The detection limits of methyl parathion and carbofuran were $5\times10^{-14}$ M and $5\times10^{-13}$ M, respectively. The two linear ranges indicated that the biosensor was more sensitive for detecting low concentration of pesticides than high concentration of pesticides. The performances of the biosensor were compared with other AChE biosensors reported by literatures (Table 1).

Inhibition effects were also investigated by DPV. As shown in Fig. S8, the response of the biosensor before and after 6 min incubation in $10^{-12}$, $10^{-11}$, $10^{-10}$, $10^{-9}$ and $10^{-8}$ M carbofuran, the peak currents (curves b–f) dramatically decreased compared with that on the control (curve a), and the decrease in peak current increased with the increasing concentration of carbofuran. The calibration plot of inhibition percentage versus carbofuran

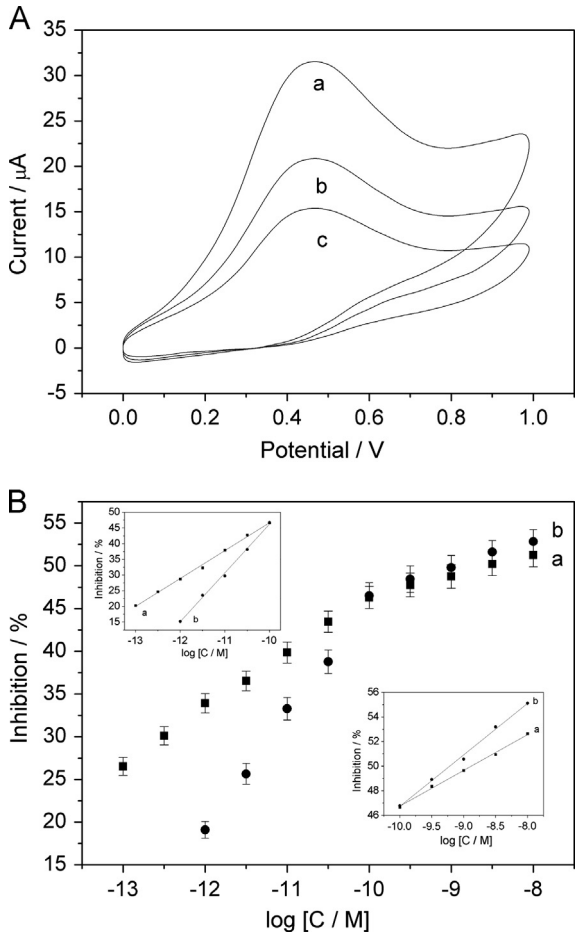


**Fig. 4.** (A) Amperometric response of NF/AChE–CS/$SnO_2$ NPs–CGR–NF/GCE in 0.1 M PBS containing 0.5 mM ATCl by CV after incubation with 0 (a), $10^{-12}$ M (b) and $10^{-8}$ M (c) methyl parathion for 6 min; and (B) inhibition curves of NF/AChE–CS/$SnO_2$ NPs–CGR–NF/GCE biosensor for methyl parathion (a) and carbofuran (b) determination by CV.

**Table 1**
Comparisons of the response of the biosensor for detection of pesticides with other biosensor based on AChE.

| Sample | Electrode | Liner range (M) | Detection limit (M) | References |
|---|---|---|---|---|
| Methyl parathion | AChE–LDHs[a]/GCE | $1.9\times10^{-8}$–$1.1\times10^{-6}$; $1.1\times10^{-6}$–$1.5\times10^{-5}$ | $2.3\times10^{-9}$ | Gong et al. (2013) |
| | AChE–SF[b]/MWNTs[c]/GCE | $3.5\times10^{-6}$–$2.0\times10^{-3}$ | $5.0\times10^{-7}$ | Xue et al. (2012) |
| | NF/AChE–CS/$SnO_2$NPs–CGR–NF/GCE | $10^{-13}$–$10^{-10}$; $10^{-10}$–$10^{-8}$ | $5.0\times10^{-14}$ | This work |
| Carbofuran | AChE/PAMAM[d]–Au/CNTs/GCE | $4.5\times10^{-9}$–$9.0\times10^{-8}$ | $4.0\times10^{-9}$ | Qu et al. (2010) |
| | AChE–TCNQ[e]/SPE[f] | $9.0\times10^{-10}$–$7.5\times10^{-7}$ | $9.0\times10^{-10}$ | Nunes et al. (2004) |
| | NF/AChE–CS/$SnO_2$NPs–CGR–NF/GCE | $10^{-12}$–$10^{-10}$; $10^{-10}$–$10^{-8}$ | $5.0\times10^{-13}$ | This work |

[a] Layered double hydroxides.
[b] Silk fibroin.
[c] Multiwalled carbon nanotubes.
[d] Polyamidoamine.
[e] 7,7,8,8-tetracyanoquinodimethane.
[f] Screen-printed electrode.

concentration was shown in Fig. S9. Linear equations of carbofuran were $I(\%)=13.71\ \log C+180.75$ ($r=0.997$) from $10^{-12}$ to $10^{-10}$ M and $I(\%)=5.23\ \log C+100.85$ ($r=0.996$) from $10^{-10}$ to $10^{-8}$ M with the detection limit of $5.0\times10^{-13}$ M. The result indicated that DPV analysis had high resolution and sensitivity than CV.

### 3.7. Interference study

The interfering signal due to the most common electroactive species was studied. The signal for a 0.5 mM ATCl was compared with the signal obtained in the presence of the interfering species. The test results showed that no noticeable changes in amperometric responses were detected in the presence of glucose (0.5 mM), citric acid (0.5 mM), oxalic acid (0.5 mM), $PO_4^{3-}$ (0.5 mM), $SO_4^{2-}$ (0.5 mM), $NO_3^-$ (0.5 mM), Cu(II) (0.5 mM) and Pb(II) (0.5 mM) at the present operating potential in this system. However, 0.5 mM of p-nitrophenol, 0.5 mM of nitrobenzene, 0.5 mM of p-nitroaniline, 0.5 mM of trinitrotoluene, 0.5 mM of toluene, 0.5 mM of p-toluenesulfonic acid and 0.5 mM of Hg(II) severely interfered with the determination. Besides, equal concentration of methyl parathion and carbofuran interfered with each other for the determination. The interference study results were showed in Fig. S10.

### 3.8. Repeatability, reproducibility and stability studies

The RSD of intra-assay and inter-assay were found to be 3.6% and 5.5% as shown in Table S1 and Table S2, respectively. When the enzyme electrode was not in use, it was stored at 4 °C in dry condition. No obvious decrease in the response of ATCl was observed in the first 10-day storage. After a 30-day storage period, the biosensor retained 90% of its initial amperometric response, indicating the acceptable stability of biosensor. The variation of amperometric response of the biosensor with time was showed in Fig. S11.

### 3.9. Analysis of real samples

To investigate the accuracy of an analytical method, spike recovery is a useful tool. The variability was low if there were no interferences or matrix effects, so a recovery close to 100% was expected. Table S3 showed the results obtained by analysis of these spiked samples. The recoveries of apple, cabbage and lake water samples were observed in the range of 92.0%–107.5%, which demonstrated low matrix effect on the amperometric response. The low relative standard deviations for methyl parathion and carbofuran demonstrated the high precision of analysis.

## 4. Conclusion

In this paper, combining the advantageous characteristics of CGR, $SnO_2$ NPs and NF, the $SnO_2$ NPs–CGR–NF nanocomposites have been prepared. The $SnO_2$ NPs–CGR–NF nanocomposites with excellent conductivity, catalysis and biocompatibility offered an extremely hydrophilic surface that was favorable for AChE adhesion, biological activity maintenance and conductivity between AChE and modified electrode. CS was used as to immobilize the AChE on $SnO_2$ NPs–CGR–NF/GCE. NF was used as the protective membrane of the AChE biosensor to improve stability. The NF/AChE–CS/ $SnO_2$ NPs–CGR–NF biosensor has been developed. The constructed biosensor exhibited many advantages such as low applied potential, good fabrication reproducibility, acceptable stability, fast response and low detection limit. The biosensor has potential application in biomonitoring of methyl parathion and carbofuran pesticides and other organophosphate and carbamate pesticides. The method not only can be used to immobilize other enzymes to construct a range of biosensors but also may be extended to assemble other biological molecules, such as antibody, antigen and DNA for wide bioassay applications.

## Acknowledgment

Qing Zhou acknowledges support from the Research Fund for the Teacher's Program of Yunnan University (No. XT412003).

## Appendix A. Supporting information

Supplementary information associated with this article can be found in the online version at http://dx.doi.org/10.1016/j.bios.2013.04.037.

## References

Andreescu, S., Marty, J.L., 2006. Biomolecular Engineering 23, 1–15.
Chappel, S., Zaban, A., 2002. Solar Energy Materials and Solar Cells 71, 141–152.
Chen, D., Tang, L.H., Li, J.H., 2010. Chemical Society Reviews 39, 3157–3180.
Chen, D., Feng, H.B., Li, J.H., 2012. Chemical Reviews 112, 6027–6053.
Chu, D., Masuda, Y., Ohji, T., Kato, K., 2011. Chemical Engineering Journal 168, 955–958.
Fuchs, A., Schimper, H.J., Klein, A., Jaegermann, W., 2011. Energy Procedia 10, 149–154.
Gong, J.M., Guan, Z.Q., Song, D.D., 2013. Biosensors and Bioelectronics 39, 320–323.
Guo, S.J., Dong, S.J., 2011. Journal of Materials Chemistry 21, 18503–18516.
Han, S.S., Kim, H., Park, N., 2011. Journal of Physical Chemistry C 115, 24696–24701.
Han, T.H., Lee, W.J., Lee, D.H., Kim, J.E., Choi, E.Y., Kim, S.O., 2010. Advanced Materials 22, 2060–2064.
Hosea, N.A., Berman, H.A., Taylor, P., 1995. Biochemistry 34, 11528–11536.
Hummers, W.S., Offeman, R.E., 1958. Journal of the American Chemical Society 80, 1339.

Hu, Z.M., Seliskar, C.J., Heineman, W.R., 1998. Analytica Chimica Acta 369, 93–101.
Kim, H., Kim, S.W., Park, Y.U., Gwon, H., Seo, D.H., Kim, Y., Kang, K., 2010. Nano Research 3, 813–821.
Korotcenkov, G., Cho, B.K., Gulina, L., Tolstoy, V., 2009. Sensors and Actuators B 138, 512–517.
Kou, R., Shao, Y.Y., Wang, D.H., Engelhard, M.H., Kwak, J.H., Wang, J., Viswanathan, V.V., Wang, C.M., Lin, Y.H., Wang, Y., Aksay, I.A., Liu, J., 2009. Electrochemistry Communications 11, 954–957.
Kumaravel, A., Chandrasekaran, M., 2010. Journal of Electroanalytical Chemistry 638, 231–235.
Li, D., Kaner, R.B., 2008. Science 320, 1170–1171.
Li, J., Guo, S.J., Zhai, Y.M., Wang, E.K., 2009. Electrochemistry Communications 11, 1085–1088.
Li, L.M., Huang, J., Wang, T.H., Zhang, H., Liu, Y., Li, J.H., 2010. Biosensors and Bioelectronics 25, 2436–2441.
Li, M.G., Xu, S.D., Tang, M., Liu, L., Gao, F., Wang, Y.L., 2011. Electrochimica Acta 56, 1144–1149.
Liu, G.D., Lin, Y.H., 2006. Analytical Chemistry 78, 835–843.
Lu, T., Zhang, Y., Li, H., Pan, L., Li, Y., Sun, Z., 2010. Electrochimica Acta 55, 4170–4173.
Mahadeva, S.K., Kim, J., 2011. Sensors and Actuators B 157, 177–182.
Mishra, A.K., Ramaprabhu, S., 2011. Journal of Physical Chemistry C 115, 14006–14013.
Nie, R.F., Wang, J.H., Wang, L.N., Qin, Y., Chen, P., Hou, Z.Y., 2012. Carbon 50, 586–596.
Novoselov, K.S., Geim, A.K., Morozov, S.V., Jiang, D., Zhang, Y., Dubonos, S.V., Grigorieva, I.V., Firsov, A.A., 2004. Science 306, 666–669.
Nunes, G.S., Jeanty, G., Marty, J.L., 2004. Analytica Chimica Acta 523, 107–115.
Patil, S.B., Patil, P.P., More, M.A., 2007. Sensors and Actuators B 125, 126–130.
Qiu, J.D., Huang, J., Liang, R.P., 2011. Sensors and Actuators B 160, 287–294.
Qu, Y., Sun, Q., Xiao, F., Shi, G., Jin, L., 2010. Bioelectrochemistry 77, 139–144.
Seger, B., Kamat, P.V., 2009. Journal of Physical Chemistry C 113, 7990–7995.
Sheng, Q.L., Wang, M.Z., Zheng, J.B., 2011. Sensors and Actuators B 160, 1070–1077.
Stankovich, S., Dikin, D.A., Dommett, G.H.B., Kohlhaas, K.M., Zimney, E.J., Stach, E.A., Piner, R.D., Nguyen, S.T., Ruoff, R.S., 2006. Nature 442, 282–286.
Stoller, M.D., Park, S.J., Zhu, Y.W., An, J.H., Ruoff, R.S., 2008. Nano Letters 8, 3498–3502.
Sun, X.M., Liu, Z., Welsher, K., Robinson, J.T., Goodwin, A., Zaric, S., Dai, H.J., 2008. Nano Research 1, 203–212.
Videira, R.A., Antunes-Madeira, M.C., Lopes, V.I.C.F., Madeira, V.M.C., 2001. Biochimica et Biophysica Acta (1511), 360–368.
Wang, Y., Zhang, S., Du, D., Shao, Y.Y., Li, Z.H., Wang, J., Engelhard, M.H., Li, J.H., Lin, Y.H., 2011a. Journal of Materials Chemistry 21, 5319–5325.
Wang, Y., Li, Z.H., Wang, J., Li, J.H., Lin, Y.H., 2011b. Trends in Biotechnology 29, 205–212.
Wang, K., Liu, Q., Dai, L.N., Yan, J.J., Ju, C., Qiu, B.J., Wu, X.Y., 2011. Analytica Chimica Acta 695, 84–88.
Wang, X., Zhi, L.J., Tsao, N., Tomovic, Z., Li, J.L., Mullen, K., 2008. Angewandte Chemie International Edition 47, 2990–2992.
Wen, Z.H., Wang, Q., Zhang, Q., Li, J.H., 2007. Advanced Functional Materials 17, 2772–2778.
Wu, J.B., Becerril, H.A., Bao, Z.N., Liu, Z.F., Chen, Y.S., Peumans, P., 2008. Applied Physics Letters 92, 263302–263303.
Xiao, J., Mei, D., Li, X., Xu, W., Wang, D., Graff, G.L., Bennett, W.D., Nie, Z., 2011. Nano Letters 11, 5071–5078.
Xue, R., Kang, T.F., Lu, L.P., Cheng, S.Y., 2012. Applied Surface Science 258, 6040–6045.
Yang, X.Y., Zhang, X.Y., Ma, Y.F., Huang, Y., Wang, Y.S., Chen, Y.S., 2009. Journal of Materials Chemistry 19, 2710–2714.
Yao, J., Shen, X., Wang, B., Liu, H., Wang, G., 2009. Electrochemistry Communications 11, 1849–1852.
Yoo, E., Kim, J., Hosono, E., Zhou, H.S., Kudo, T., Honma, I., 2008. Nano Letters 8, 2277–2282.
Zheng, D., Vashist, S.K., Al-Rubeaan, K., Luong, J.H.T., Sheu, F.S., 2012. Talanta 99, 22–28.